Received: 7 April 2019 | Revised: 30 April 2019 | Accepted: 13 May 2019
DOI: 10.1002/inf2.12015

SPECIAL ISSUE ARTICLE

WILEY

# Interstitial copper-doped edge contact for n-type carrier transport in black phosphorus

Ziyuan Lin[1] | Jingli Wang[1] | Xuyun Guo[1] | Jiewei Chen[1] | Chao Xu[1] | Mingqiang Liu[2] | Bilu Liu[2] | Ye Zhu[1] | Yang Chai[1]

[1]Department of Applied Physics, The Hong Kong Polytechnic University, Kowloon, Hong Kong, People's Republic of China

[2]Shenzhen Geim Graphene Center (SGC), Tsinghua-Berkeley Shenzhen Institute (TBSI), Tsinghua University, Shenzhen, Guangdong, People's Republic of China

**Correspondence**
Yang Chai, Department of Applied Physics, The Hong Kong Polytechnic University, Hung Hom, Kowloon, Hong Kong, People's Republic of China.
Email: ychai@polyu.edu.hk

**Funding information**
Research Grants Council, University Grants Committee, Grant/Award Number: PolyU 152145/15E; Hong Kong Polytechnic University, Grant/Award Numbers: SB79, 15E

**Abstract**
Black phosphorus (BP) has been shown as a promising two-dimensional (2D) material for electronic devices owing to its high carrier mobility. To realize complementary electronic circuits with 2D materials, it is important to fabricate both n-type and p-type transistors with the same channel material. By engineering the contact region with copper (Cu)-doped BP, here we demonstrate an n-type carrier transport in BP field-effect transistors (FETs), which usually exhibit strongly p-type characteristics. Cu metal atoms are found to severely penetrate into the BP flakes, which forms interstitial Cu ($Cu_{int}$)-doped edge contact and facilitates the electron transport in BP. Our BP FETs in back-gated configuration exhibit n-type dominant characteristics with a high electron mobility of ~ 138 $cm^2 V^{-1} s^{-1}$ at room temperature. The Schottky barrier height for electrons is relatively low because of the edge contact between $Cu_{int}$-doped BP and pristine BP channel. The contact doping of BP by highly mobile Cu atoms gives rise to n-type transport property of BP FETs. Furthermore, we demonstrate a p-n junction on the same BP flake with asymmetric contact. This strategy on contact engineering can be further extended to other 2D materials.

**KEYWORDS**
black phosphorus (BP), carrier type, contact, doping, two-dimensional (2D) materials

## 1 | INTRODUCTION

Two-dimensional (2D) layered semiconductors have shown great promise for future nanoelectronics due to their ultrathin body thickness, dangling-bond-free surface, and reasonably good carrier mobility.[1-5] Among the monoelemental 2D materials, black phosphorus (BP), also referred to as phosphorene, received significant attention for its atomic scale smoothness, widely tunable direct band gap (ranging from 0.3~0.39 eV for bulk to 1.5~2.0 eV for monolayer), and high hole mobility ($10^2$-$10^3$ $cm^2 V^{-1} s^{-1}$) at room temperature.[6-8] The BP field-effect transistors (FETs) exhibit an ON/OFF ratio about $10^5$ and a hole mobility up to $10^3$ $cm^2 V^{-1} s^{-1}$.[6] In contrast to molybdenum disulfide ($MoS_2$, one of the most studied 2D semiconductors), BP is predicted to have higher carrier mobility for both electrons and holes, which facilitates its application for complementary logic circuits.[7] Although the pristine BP has no dominant preference for carrier type, the extensively reported BP transistors exhibit p-type dominant transport property due to the Fermi level pinning at the contacts and the suppressed electron transport caused by oxygen and moisture exposure.[8-10] To

Ziyuan Lin and Jingli Wang authors contributed equally to this work.

This is an open access article under the terms of the Creative Commons Attribution License, which permits use, distribution and reproduction in any medium, provided the original work is properly cited.
© 2019 The Authors. *InfoMat* published by John Wiley & Sons Australia, Ltd on behalf of UESTC.

realize low-power complementary circuits, it is important to fabricate both p-type and n-type transistors with the same channel materials.[11]

Contact engineering and surface doping have been applied to modulate the carrier type and achieve complementary 2D material transistors.[12-17] In recent studies, n-type BP transistors were fabricated by utilizing contact metals with low work function, such as aluminum (Al) and scandium (Sc).[12,13] The n-type characteristic is mainly attributed to the energy level match between the conduction band of few-layer BP ($E_c$ ~ 4.1 eV) and the work function of contact metal electrode ($\Phi_{Al}$ ~ 4.0 eV, $\Phi_{Sc}$ ~ 3.5 eV). These low-work-function metal contacts hold the BP Fermi level close to the conduction band minimum with low Schottky barrier height (SBH) for electrons. Except utilizing low-work-function metals, surface charge transfer offers another way for modulation doping.[14-19] Surface functionalization with cesium carbonate ($Cs_2CO_3$) is reported to strongly electron dope BP, where the BP FETs exhibit transition from ambipolar to n-type transport property with the increase of the thickness of $Cs_2CO_3$.[14] Copper (Cu) adatoms can also act as electron donor and n-dope BP, which greatly shifts the Fermi level of BP toward the conduction band and modulates the

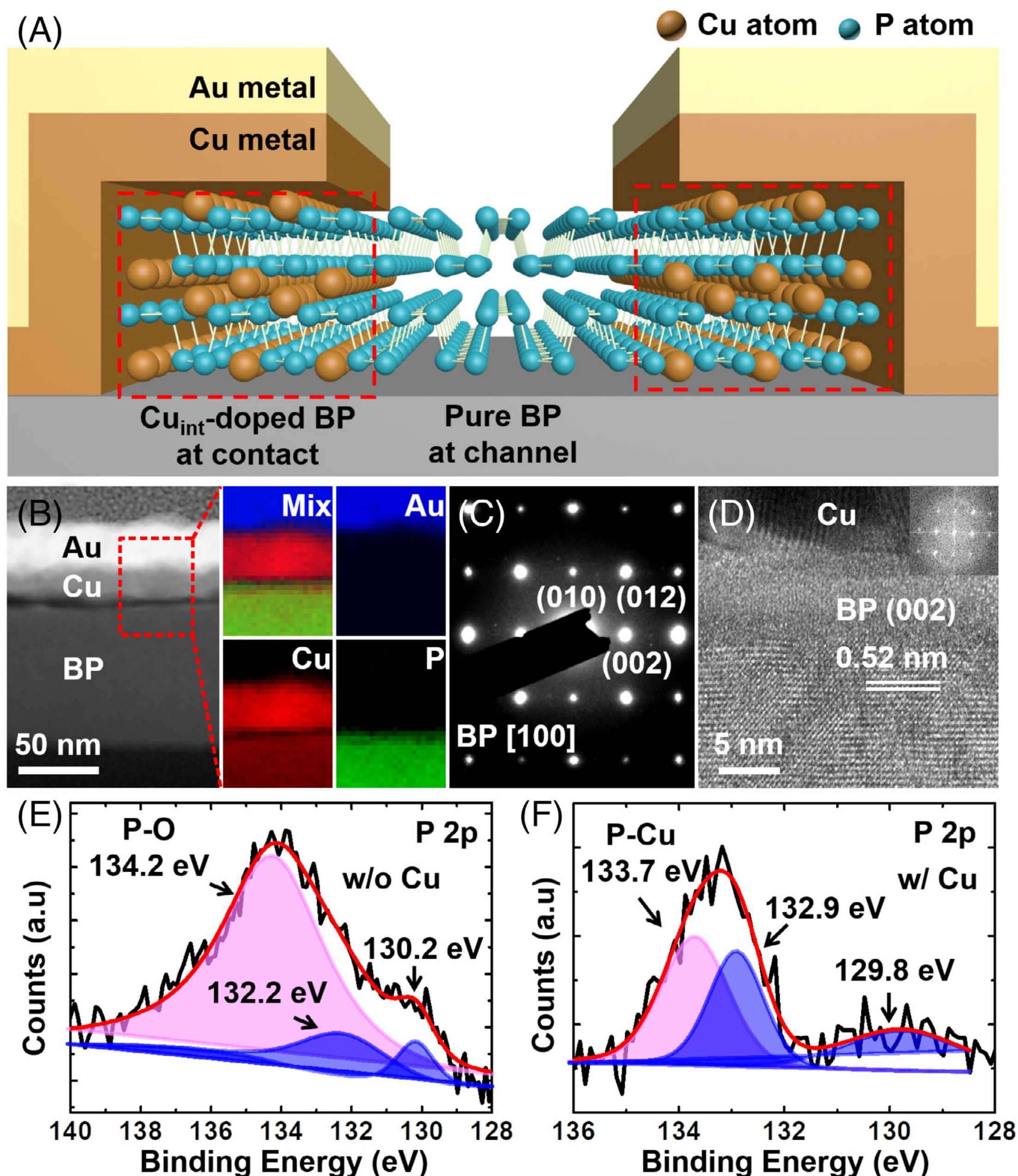


**FIGURE 1** A, Cross-sectional schematic of $Cu_{int}$-doped contact of BP FETs. B, Cross-sectional STEM of Au/Cu/BP flake and the corresponding elemental mapping images. C, SAED pattern of the $Cu_{int}$-doped BP flake. D, HRTEM image of the $Cu_{int}$-doped BP. The inset shows the corresponding FFT pattern. E, F, XPS spectra of BP flakes without and with Cu coating

polarity of BP channel from p-type to n-type.[15] Also, metal Cu is proposed to make excellent contact with BP.[20] However, the Cu contact for BP FETs has not been experimentally demonstrated. In addition, the contact doping effect from Cu is also not studied, which requires further investigation.

In this work, we first investigated the interface between BP flake and Cu electrode. Highly diffusive Cu atoms migrate into the BP flake and intercalate between BP layers without changing the crystal structure of BP. The Fermi level is greatly shifted toward the conduction band of BP after the Cu penetration. The BP with interstitial Cu ($Cu_{int}$) has metallic-like electrical property, and forms edge contact to pure BP channel. Through this $Cu_{int}$-doped edge contact, we demonstrated n-type dominant BP transistors with high electron mobility of ~ 138 $cm^2\ V^{-1}\ s^{-1}$ at room temperature. The current density can reach 58 μA/μm. This n-type transport property is attributed to n-doping induced by the penetration of highly mobile Cu atoms at the contact region.

## 2 | RESULTS AND DISCUSSION

### 2.1 | Cu diffusion in BP

Figure 1A shows the cross-sectional schematic of the BP FET with Cu contacts. The contact between metal and semiconductor greatly affects the contact resistance and carrier type of devices.[11] As the highly diffusive Cu may change the contact with BP, it is important to understand the interface between BP flake and Cu electrode. The Raman spectrum of the BP flake in Figure S1 shows three sharp peaks at 361 $cm^{-1}$, 438 $cm^{-1}$, and 466 $cm^{-1}$, corresponding to $A^1_g$, $B_{2g}$, and $A^2_g$ vibration modes. These values are consistent with the previous studies, confirming the nature of the BP flake.[8,21,22] To facilitate the cross-sectional TEM characterization, we chose the BP flake with a relatively large thickness. Figure 1B presents the cross-sectional scanning transmission electron microscopy (STEM) image of a BP flake covered with 30-nm-thick Cu layer and 30-nm-thick Au layer, which shows clear interfaces between the Au/Cu/BP/$SiO_2$ stacks. The electron energy loss spectroscopy (EELS) mapping of elements Au, Cu, and P qualitatively reveals the chemical distribution and provides detailed sight of the BP/Cu interface. As shown in the EELS elemental analysis, the Cu penetrates the BP flake and exhibits relatively homogeneous distribution. The corresponding line scan of EELS mapping (Figure S2) presents a slight decrease of Cu signal as there is an increase in penetration depth inside BP, thus indicating that the Cu amount gradually decreases beneath the contact

To identify the doping configuration of Cu atoms, we performed detail characterization of the crystal structure of the Cu-penetrated BP. Figure 1C presents selected area electron diffraction (SAED) of the Cu-penetrated BP flake. The well-indexed diffraction pattern is in accordance with the pristine BP crystal (ICDD-PDF No. 76-1963), indicating that the BP flake maintains its orthorhombic crystal structure even after the Cu penetration. The high-resolution TEM (HRTEM) image (Figure 1D) also clearly shows the interlayer lattice of the BP flake. The interlayer distance of BP with Cu dopant is 0.52 nm, which is still consistent with the reported values (~ 0.524 nm) of pure BP.[23,24] The inserted fast Fourier transform (FFT) pattern is identical with that of pristine BP (Figure S3). The unchanged crystal structure of the BP flake after the Cu penetration indicates the Cu dopant atoms act as interstitial atoms in the BP crystal rather than forming compounds with BP. The atom size of Cu ($r_{Cu}$ ~ 0.14 nm) is smaller than the interlayer distance (0.52 nm) of BP flakes and larger than "pore" size (<0.1 nm) of BP plane, which suggests that the Cu atoms are intercalated between the BP layers.[24] We deduce that the Cu intercalation begins at the edge sites or surface defects of the BP flake during the metal evaporation when the high energy and highly diffusive evaporated Cu atoms facilitate the intercalation process.[25-27] The intercalated Cu atoms propagate along the interlayer between BP planes, which results in BP with interstitial Cu ($Cu_{int}$) between BP layers. While the BP beneath the Cu contact experiences the $Cu_{int}$ doping, the BP at channel maintains its pure characteristics. Figure S4A presents the TEM image of the BP flakes at the edge of Cu/Au layers. The undoped BP at channel is magnified in Figure S4B and the corresponding EELS element mapping confirms the absence of Cu in the BP layer, which indicated that the doping of $Cu_{int}$ is limited in the contact region.

Figure 1E,F presents the XPS spectra of BP without and with Cu coating. Pristine BP shows a strong peak at 134.2 eV, corresponding to the P-O bonds, which indicates oxidization of BP. In contrast, the peak at 133.7 eV observed from BP with Cu coating can be attributed to the interaction between Cu and BP. In each layer of BP, the lone pair electrons of phosphorus atoms interact with each other, forming conjugated π bonds at the surface and interlayer. During the metal evaporation, the evaporated Cu atoms have negative formation energy with the conjugated π bond of BP, indicating the spontaneous electron interaction between Cu and BP at the surface and interlayer.[16] The thermally favored formation of Cu-P interactions also promotes the penetration of $Cu_{int}$ between BP layers

Although the $Cu_{int}$ dopant negligibly changes the crystal structure of BP flakes, it greatly affects the electrical property of few-layer BP. We studied the effect of $Cu_{int}$ on the band structure of few-layer BP based on density functional theory (DFT). Figure S5A,B shows the atomic configuration of pristine BP and $Cu_{int}$-doped BP. For pristine BP, the band structure in

Figure S5C clearly shows that the Fermi level lies in the middle of the bandgap. In contrast, Figure S5D shows that the Fermi level of BP with $Cu_{int}$ is greatly shifted toward the conduction band, which is in agreement with n-doping effects of Cu adatoms.[15] The Cu atoms donate electrons from the outmost 4s shell, which induces the n-doping effect of $Cu_{int}$. In addition, the bandgap of BP with $Cu_{int}$ is 0.2 eV smaller than that of the pristine BP, indicating the transition from semiconductor to semi-metal of BP after Cu penetration. The changed band structure suggests the metallic-like behavior of $Cu_{int}$-doped BP, which consequently changes the contact of BP FETs with Cu electrodes. The calculated work function of the metallic like $Cu_{int}$-doped BP is 3.59 eV, which changes the energy level match between BP and Cu contact.

As illustrated in Figure 1A, the BP beneath the Cu contact experiences great n-doping effect of Cu from metal electrode. These penetrated Cu atoms act as interstitial dopants and maintain the crystal structure of BP at contacts, which allows excellent edge contact to pristine BP channel. In addition, although the $Cu_{int}$-doped BP does not change its orthorhombic structure, the electrical structure is greatly changed. The metallic-like electrical property of $Cu_{int}$-doped BP further assures the excellent edge contact. The $Cu_{int}$-doped BP edge contact is contributed to the achievement of n-type BP FETs, providing another way to control carrier type beyond the methods with low-work-function metal contact and surface doping.

## 2.2 | BP FETs with Cu contact

Figure 2A presents the transfer curve of a typical BP transistor with 10 nm thickness, which exhibits n-type dominant transport behavior with a high electron mobility of ~138 $cm^2 V^{-1} s^{-1}$ at room temperature. The current density can reach 58 μA/μm (Figure 2B). The n-type dominant transport property in BP FET with Cu contact reveals the obvious n-doping effect induced by the $Cu_{int}$-doped BP edge contact and the small SBH for electron. Figure S6 presents the thickness-dependent transfer curves of BP transistors. The ON/OFF ratio is reduced to 10 with the increase of BP thickness. As the thickness of BP increases, the n-branch current changes slightly, suggesting that the SBH for electron is small and nearly independent of BP thickness. The p-branch current dramatically increases by 10 times, which indicates that the considerable SBH for hole is reduced when bandgap is narrowed with the increase of BP thickness. The different change of p/n-branch current results in the transition of devices from n-type to n-type dominant ambipolar, suggesting different SBH for hole and electron. The simplified band diagram of $Cu_{int}$-doped edge contact is presented in Figure 2C. The $Cu_{int}$-doped BP has a Fermi level lying above the conduction band, which makes it act as metal. When $V_{gs} > V_T$ (threshold voltage), the $Cu_{int}$-doped BP edge contact has a small SBH for electron because the energy level matches between $Cu_{int}$-doped BP and pristine BP. In contrast, the pure Cu contact with large work function (4.65 eV) will induce large SBH for electron and hamper the electron transport. When

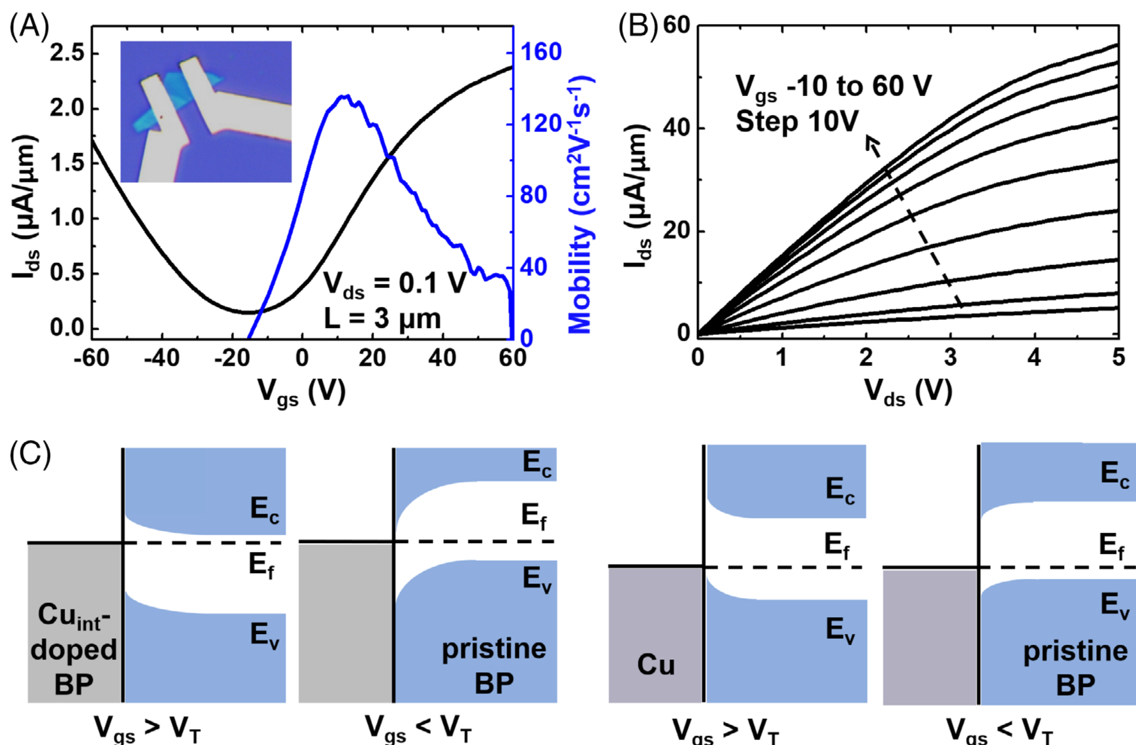


**FIGURE 2** A, Transfer curve of a typical BP FET with Cu contact exhibiting strong n-type transport property. The inset shows the corresponding optical image. B, Output curve of the n-type BP FET. C, Simplified band diagram of $Cu_{int}$-doped BP edge contact and pure Cu

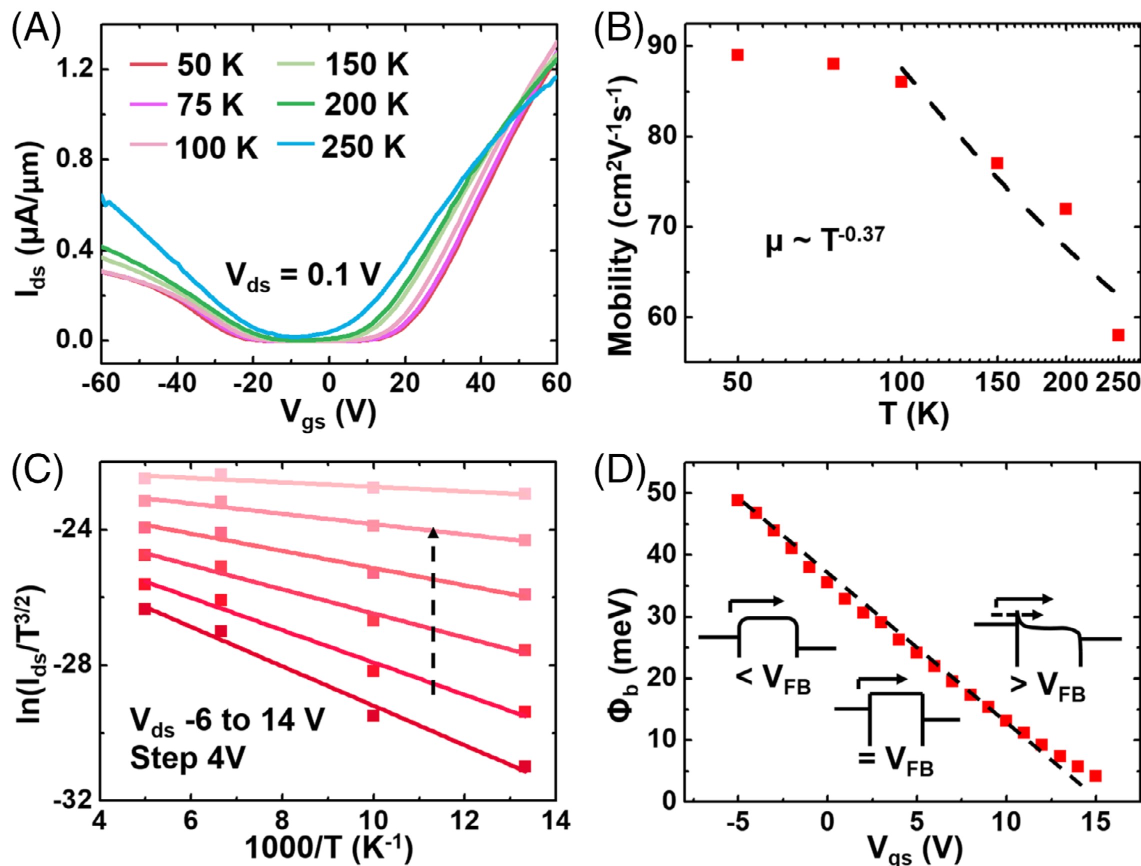


**FIGURE 3** A, Temperature-dependent transfer curves. B, Temperature-dependent mobility of BP FET. C, The Arrhenius plots for different back-gate voltages. D, The extracted Schottky barrier heights for different back-gate voltages

$V_{gs} < V_T$, the hole transport in BP with $Cu_{int}$-doped edge contact is hindered for a large SBH for hole while the pure Cu should facilitate the hole transport.[28] The $Cu_{int}$-doped edge contact changes the energy level match between pure Cu and pure BP, which achieves the n-type transport property of BP FET by providing small SBH for electron. The low work function of $Cu_{int}$-doped edge contact is benefited from the great n-doping effect of $Cu_{int}$ on BP flakes

We also performed temperature-dependent characterization of the devices to understand the barrier height at the contact region. Figure 3A shows the transfer curves of the BP transistor at various temperatures. The n-branch current of ambipolar BP FET exhibits negligible temperature dependence, which indicates a small Schottky barrier for electrons. In contrast, the p-branch current exhibits relatively large temperature dependence. With the decrease of the temperature, the p-branch current is decreased, revealing a larger Schottky barrier for holes.[9] Figure 3B presents the temperature-dependent electron mobility. As the temperature decreases from 250 to 50 K, the mobility of BP is increased from 58 $cm^2\ V^{-1}\ s^{-1}$ to 89 $cm^2\ V^{-1}\ s^{-1}$, which is attributed to the reduced phonon scattering at low temperature. In the phonon scattering region, the mobility fits the expression $\mu \sim T^{-\gamma}$, where $\mu$ is the carrier mobility and $T$ is the temperature, and the exponent $\gamma$ was extracted to be 0.37 for the devices. The output curves at different temperatures are also shown in Figure S7A (300 K) and Figure S7B (50 K). The current density exhibits a great increase from 41 μA/μm to 52 μA/μm with the decrease of temperature, confirming the reduced phonon scattering at low temperature.

We further tried to extract the SBH for electron of BP-Cu contact from temperature-dependent performance.[3] The Arrhenius plots in Figure 3C were obtained from the temperature-dependent transfer curves. The slope is associated with the barrier height at various back-gate voltages. According to thermionic theory, when the back-gate voltage is below flat-band voltage ($V_{FB}$), the thermionic emission current dominates the drain current.[28] The barrier height shows a linear relationship as a function of the gate voltage. When the back-gate voltage is larger than $V_{FB}$, thermally assisted tunneling current contributes to the drain current, which results in the nonlinear behavior between barrier height and gate voltage. At the turning point (the back-gate voltage equals to $V_{FB}$), the relationship between barrier height and the back-voltage changes from linear to nonlinear. SBH can be extracted when the back-gate voltage equals to $V_{FB}$, because thermally assisted tunneling does not contribute to the current. As shown in Figure 3D, the barrier height maintains linear relationship as a

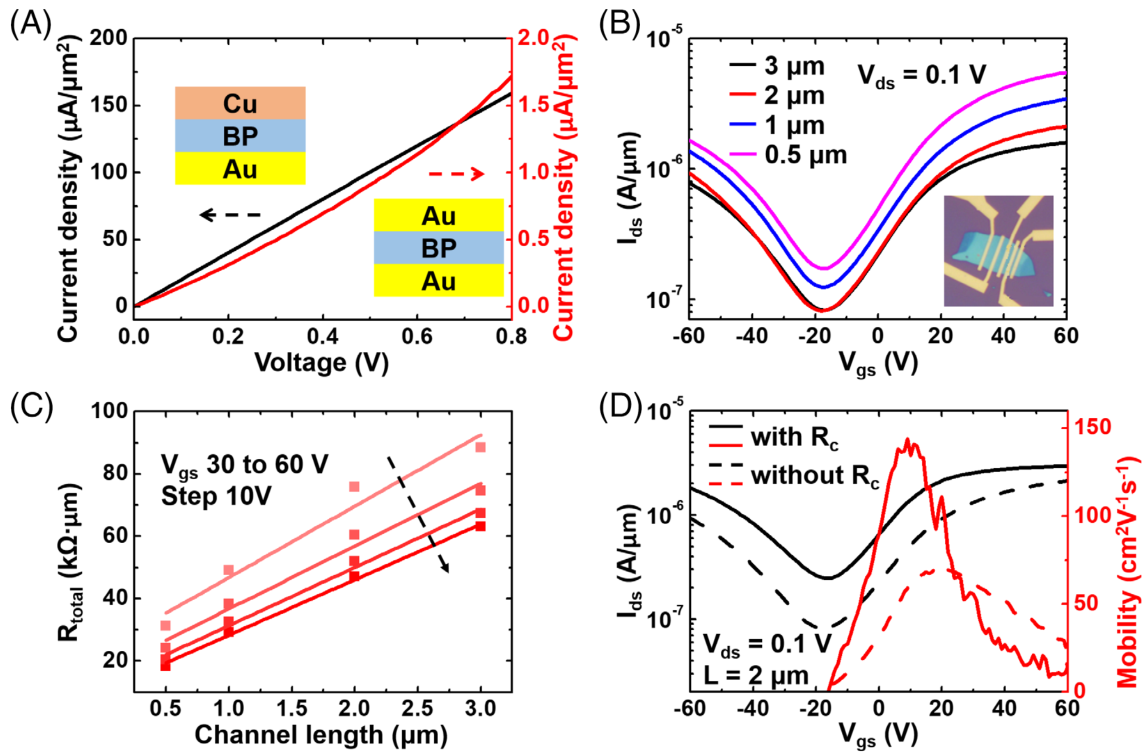


**FIGURE 4** A, Current density of vertical junction Cu/BP/Au and Au/BP/Au. B, Transfer curves of BP FET with different channel lengths. C, Total resistance vs channel length at different gate voltages. D, Transfer curve and mobility with and without contact resistance

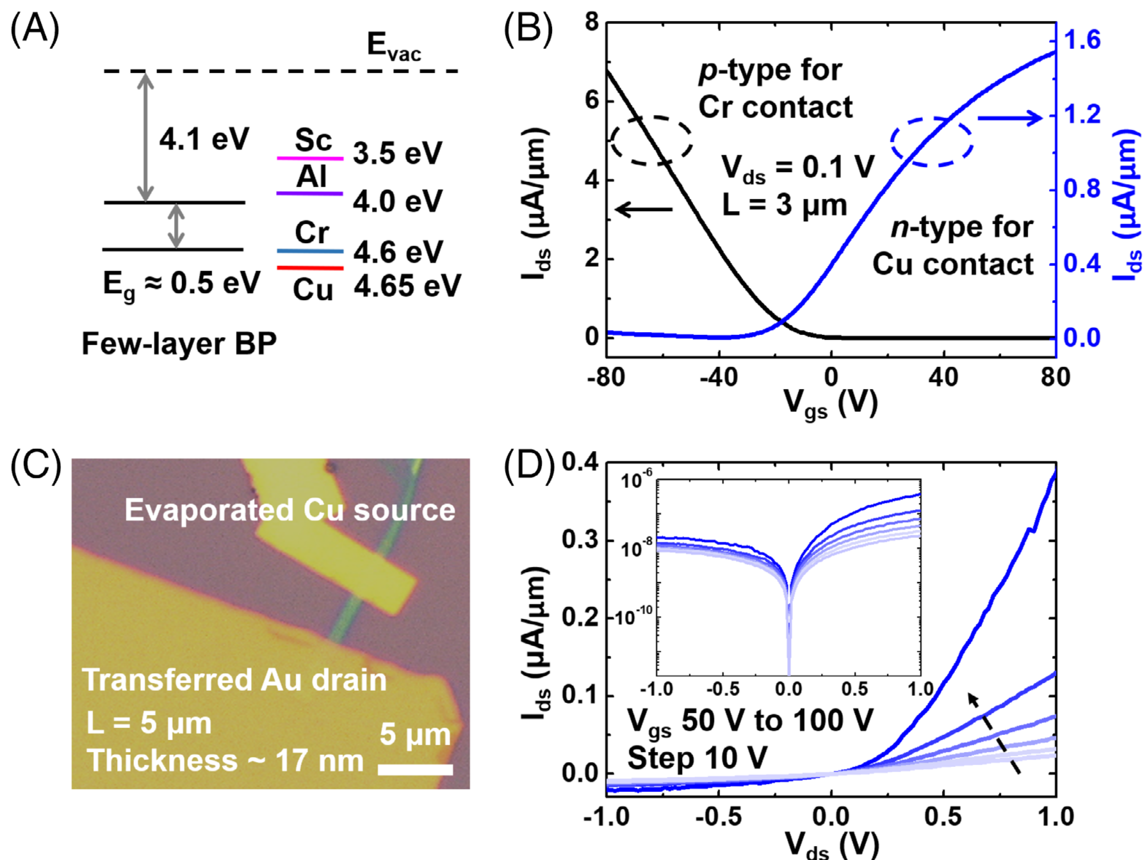


**FIGURE 5** A, Band alignment between few-layer BP and different metals. B, Transfer curves of BP FET with evaporated Cr contact and Cu contact. C, Optical image of BP p-n junction with asymmetric contact. D, Output curve of BP p-n junction. The inset shows the output curve in semilogarithmic scale

function of the gate voltage without turning point where the curve changes to nonlinear. The linear relationship without turning point suggests the negligible SBH, which is attributed to $Cu_{int}$-doped BP edge contact.

The direct edge contact between $Cu_{int}$-doped BP and pristine BP at channel induces the negligible SBH for electron and promotes electron transport in BP because of the energy level match between metallic-like $Cu_{int}$-doped BP and pristine BP. The metallic-like $Cu_{int}$-doped BP edge contact has a matched energy level with pure BP and small barrier height for electron, which accounts for the achievement of n-type BP FET.

In addition to providing small SBH for electron in BP, the $Cu_{int}$-doped BP also forms Ohmic contact with metal electrodes. Figure 4A shows the *I-V* curve of Cu/BP/Au vertical junction. The current exhibits linear relationship as a function of the applied voltage with the current density of 158 $\mu A/\mu m^2$, about 100 times larger than that of Au/BP/Au vertical junction (1.70 $\mu A/\mu m^2$). The linear *I-V* curve of Cu/BP/Au indicates the metallic characteristics of the junction, while the nonlinear *I-V* relationship of Au/BP/Au suggests non-Ohmic contact. The linear relationship and high current density of Cu/BP/Au result from the $Cu_{int}$ doping during metal evaporation process. The penetrated Cu in BP changes the electrical property of BP to metallic-like behavior, which is consistent with our DFT calculation. The Ohmic contact between $Cu_{int}$-doped BP and metal electrodes benefits n-type BP FET with low contact resistance.

Transfer length method (TLM) is usually utilized to measure the contact resistance of devices. Figure 4B presents the transfer curves of BP FETs with different channel lengths, showing similar off-state voltages for different channel lengths. The inset image shows the 10-nm-thick BP device for TLM measurement. The total resistance can be calculated from the transfer curves with different channel lengths and gate voltages. Figure 4C shows the relationship between the total resistance and channel length at different gate voltages. The contact resistance can be extracted from the intercept of relationship between total resistance and channel length. The extracted contact resistance is about 5 kΩ μm at a gate voltage of 60 V, which is comparable with that of p-type FET based on BP (7.5 kΩ μm) and that of n-type FETs based on other 2D materials (like $MoS_2$, 1 kΩ μm).[29,30] After the contact resistance is excluded, we replot the transfer curve in Figure 4D. The effective electron mobility calculated from the new transfer curve is 148 $cm^2\ V^{-1}\ s^{-1}$, higher than the previous value (72 $cm^2\ V^{-1}\ s^{-1}$) without excluding contact resistance. The relatively low contact resistance of Cu-BP contact benefits from the $Cu_{int}$-doped BP edge contact. The metallic-like $Cu_{int}$-doped BP has an excellent contact with metal electrodes and a matched energy level with pure BP at channel, which produces negligibly low barrier height at the contact and subsequently results in the relatively low contact resistance of BP FET with Cu contact.

## 2.3 | p-n diode by asymmetric contact engineering

We further compared with the performance of BP transistors with chromium (Cr) contact. Figure 5A presents the schematic band alignment between several metals (Sc, Al, Cr, and Cu) and few-layer BP. The band gap of few-layer BP is assumed to be ~0.5 eV.[12,13] As shown in Figure 5A, the Cr metal has a work function of 4.6 eV, which is close to that of Cu metal (4.65 eV). The transfer (Figure 5B) and output curves (Figure S8) indicate strongly unipolar p-type characteristics of BP transistors with Cr contact, which is consistent with the band alignment of Cr-BP. The p-type BP FET with Cr contact exhibits an ON/OFF ratio of $10^3$ and a high hole mobility of 180 $cm^2\ V^{-1}\ s^{-1}$. In comparison, the BP FET with Cu contact exhibits n-type transport property with same channel length. As compared in Figure 5B, the BP transistors with Cr and Cu contact metals exhibit different types of carrier transport in spite of their similar work function, suggesting different carrier-type control mechanisms. The p-type BP FET with Cr contact is attributed to the band alignment of Cr-BP and Fermi level pinning effect. On the other hand, the work function of Cu is about 4.65 eV and much higher than that of Al (4.0 eV) and Sc (3.5 eV) utilized as metal contact for reported *n*-type BP FETs. The work function value of Cu cannot match well with the conduction band edge for few-layer BP flakes (4.1 eV) but is close to the value of Cr. Sc and Al contacts achieve *n*-type BP FETs for their low work function. The carrier type control is similar to Cr contact, which achieves p-type BP FETs. Cu contact achieves *n*-type transport with similar work function to that of Cr, indicating different carrier type control mechanisms of Cu contact. The $Cu_{int}$-doped edge contact changes the energy level match as the metal-like $Cu_{int}$-doped BP has a Fermi level above the conduction band of BP, which gives rise to small SBH for electron. The contact doping promotes electron transport due to the excellent edge contact between the highly n-doped BP with $Cu_{int}$ and pristine BP.

Based on contact engineering, we further constructed a p-n junction with asymmetric contact (Au and Cu electrodes on two sides) on the same BP flakes. The BP transistors with Au electrodes have p-type characteristics (Figure S9),[31] which allows forming p-n junction with Cu electrodes. Figure 5C shows the optical image of the p-n junction based on BP with Au and Cu contacts. The Cu electrode as source was patterned by electron beam lithography while the Au electrode as drain was transferred and aligned on the BP flake.[28] Figure 5D presents the output curve of the p-n

junction. The device shows rectification behavior, with a rectification ratio of about 100.

## 3 | CONCLUSIONS

In this work, n-type dominant BP transistors with Cu contact were demonstrated. The interface between Cu and BP is contributed to the n-type transport property of BP FET. The contact metal Cu experiences penetration to BP flakes during metal evaporation, resulting in BP with interstitial Cu at the contact region. The $Cu_{int}$ n-dopes the BP and shifts the Fermi level into conduction band without changing the crystal structure of BP, which benefits the excellent $Cu_{int}$-doped BP edge contact with channel pure BP. The metallic-like $Cu_{int}$-doped edge contact also changes the energy level match between BP and Cu, which gives rise to a negligible SBH for electron and promotes electron transport. The BP transistors with Cu contact exhibit n-type dominant transport characteristics although the Cu has a relatively large work function. The devices exhibit a high electron mobility of ~ 138 $cm^2\ V^{-1}\ s^{-1}$. Although this work focuses on the Cu contact on BP, due to the highly mobile Cu atoms, other new emerging 2D material, like tellurene, may have similar responses to Cu contact and exhibit different transport properties rather than the determination by band alignment between metal electrode and semiconducting channel.

## 4 | EXPERIMENTAL SECTION

### 4.1 | Cross-sectional TEM sample preparation and characterization

The BP flake was mechanically exfoliated on silicon substrates with 300-nm-thick $SiO_2$. Cu of 30 nm and Au of 30 nm were then deposited onto the BP flakes by using a thermal evaporator. Afterward, the cross-sectional sample was prepared by using a multiBeam SEM-FIB system (JEOL Model JIB-4501), operated at 30 keV $Ga^+$, equipped with a platinum (Pt) deposition cartridge. To minimize the ion-beam damage, the interested area was first protected by a ~100 nm platinum layer by using low-voltage (5 kV) electron beam deposition. After that, a several micrometer-thick platinum layer was deposited using the gallium ion beam and then milled to <100-nm-thick lamella gradually. Finally, the thin lamella was ex situ lifted out to the Quantifoil holey carbon Cu grid by using a glass needle. TEM and STEM were performed using a JEOL JEM-2100F TEM/STEM (Tokyo, Japan) operated at 200 kV, equipped with an Oxford INCA EDS detector and a Gatan Enfina electron spectrometer for elemental mapping. EELS spectrum imaging was conducted under 200 kV accelerating voltage with an optimal convergence angle of 13 mrad. Energy dispersion of 0.7 eV per channel and a collection angle of 21 mrad were set up for EELS; HAADF images were acquired with an inner angle of 89 mrad simultaneously.

### 4.2 | Device fabrication and electrical measurement

We fabricated back-gated FETs based on few-layer BP flakes. The BP flakes were first mechanically exfoliated onto 300-nm $SiO_2$ dielectric on highly doped Si substrates, and then coated with poly(methyl methacrylate) resist for lithography process. The source and drain electrodes were patterned by electron beam lithography. Afterward, 15 nm Cu and 40 nm Au were deposited using a thermal evaporator at a base pressure of $1 \times 10^{-6}$ Torr. The devices were fabricated after lift-off process. The electrical measurements on these devices were conducted in a probe station (Lake Shore low-temperature *I-V* probe station).

## ACKNOWLEDGMENTS

This work is supported by the Research Grant Council of Hong Kong (PolyU 152145/15E and 15305718) and the Hong Kong Polytechnic University (G-YBPS, G-SB79 and 1-ZE6G). X.G. and Y.Z. thank Dr. Wei Lu for optimizing the JEOL JEM-2100F microscope.

## CONFLICT OF INTEREST

The authors declare no conflict of interest.

## ORCID

*Yang Chai* https://orcid.org/0000-0002-8943-0861

## REFERENCES

1. Liu H, Du Y, Deng Y, Ye PD. Semiconducting black phosphorus: synthesis, transport properties and electronic applications. *Chem Soc Rev*. 2015;44:2732-2743.
2. Qiu H, Pan L, Yao Z, Li J, Shi Y, Wang X. Electrical characterization of back-gated bi-layer $MoS_2$ field-effect transistors and the effect of ambient on their performances. *Appl Phys Lett*. 2012;100:123104.
3. Wang J, Yao Q, Huang CW, et al. High mobility $MoS_2$ transistor with low Schottky barrier contact by using atomic thick h-BN as a tunneling layer. *Adv Mater*. 2016;28:8302-8308.
4. Zhao Y, Qiao J, Yu P, et al. Extraordinarily strong interlayer interaction in 2D layered $PtS_2$. *Adv Mater*. 2016;28:2399-2407.
5. Lin Z, Zhao Y, Zhou C, et al. Controllable growth of large-size crystalline $MoS_2$ and resist-free transfer assisted with a Cu thin film. *Sci Rep*. 2015;5:18596.
6. Li L, Yu Y, Ye GJ, et al. Black phosphorus field-effect transistors. *Nat Nanotechnol*. 2014;9:372-377.
7. Qiao J, Kong X, Hu Z-X, Yang F, Ji W. High-mobility transport anisotropy and linear dichroism in few-layer black phosphorus. *Nat Commun*. 2014;5:4475.

8. Liu H, Neal AT, Zhu Z, et al. Phosphorene: an unexplored 2D semiconductor with a high hole mobility. *ACS Nano*. 2014;8:4033-4041.
9. Li L, Engel M, Farmer DB, Han S-J, Wong H-SP. High-performance p-type black phosphorus transistor with scandium contact. *ACS Nano*. 2016;10:4672-4677.
10. Du Y, Liu H, Deng Y, Ye PD. Device perspective for black phosphorus field-effect transistors: contact resistance, ambipolar behavior, and scaling. *ACS Nano*. 2014;8:10035-10042.
11. Zhao Y, Xu K, Pan F, Zhou C, Zhou F, Chai Y. Doping, contact and interface engineering of two-dimensional layered transition metal dichalcogenides transistors. *Adv Funct Mater*. 2017;27:1603484.
12. Perello DJ, Chae SH, Song S, Lee YH. High-performance n-type black phosphorus transistors with type control via thickness and contact-metal engineering. *Nat Commun*. 2015;6:7809.
13. Wang C-H, Incorvia JAC, McClellan CJ, et al. Unipolar n-type black phosphorus transistors with low work function contacts. *Nano Lett*. 2018;18:2822-2827.
14. Xiang D, Han C, Wu J, et al. Surface transfer doping induced effective modulation on ambipolar characteristics of few-layer black phosphorus. *Nat Commun*. 2015;6:6485.
15. Koenig SP, Doganov RA, Seixas L, et al. Electron doping of ultrathin black phosphorus with cu adatoms. *Nano Lett*. 2016;16:2145-2151.
16. Guo Z, Chen S, Wang Z, et al. Metal-ion-modified black phosphorus with enhanced stability and transistor performance. *Adv Mater*. 2017;29:1703811.
17. Zheng Y, Hu Z, Han C, et al. Black phosphorus inverter devices enabled by in-situ aluminum surface modification. *Nano Res*. 2019;12:531-536.
18. Xu K, Wang Y, Zhao Y, Chai Y. Modulation doping of transition metal dichalcogenide/oxide heterostructures. *J Mater Chem C*. 2017;5:376-381.
19. Zhou C, Zhao Y, Raju S, et al. Carrier type control of $WSe_2$ field-effect transistors by thickness modulation and $MoO_3$ layer doping. *Adv Funct Mater*. 2016;26:4223-4230.
20. Gong K, Zhang L, Ji W, Guo H. Electrical contacts to monolayer black phosphorus: a first-principles investigation. *Phys Rev B*. 2014;90:125441.
21. Guo Z, Zhang H, Lu S, et al. From black phosphorus to phosphorene: basic solvent exfoliation, evolution of Raman scattering, and applications to ultrafast photonics. *Adv Funct Mater*. 2015;25:6996-7002.
22. Guo Y, Zhang W, Wu H, et al. Discovering the forbidden Raman modes at the edges of layered materials. *Sci Adv*. 2018;4:eaau6252.
23. Huang Y, Qiao J, He K, et al. Interaction of black phosphorus with oxygen and water. *Chem Mater*. 2016;28:8330-8339.
24. Wang C, He Q, Halim U, et al. Monolayer atomic crystal molecular superlattices. *Nature*. 2018;555:231-236.
25. Abellán G, Neiss C, Lloret V, et al. Exploring the formation of black phosphorus intercalation compounds with alkali metals. *Angew Chem Int Ed*. 2017;56:15267-15273.
26. Cheng Y, Zhu Y, Han Y, et al. Sodium-induced reordering of atomic stacks in black phosphorus. *Chem Mater*. 2017;29:1350-1356.
27. Zhang R, Waters J, Geim AK, Grigorieva IV. Intercalant-independent transition temperature in superconducting black phosphorus. *Nat Commun*. 2017;8:15036.
28. Wang J. Steep slope p-type 2D $WSe_2$ field-effect transistors with van der Waals contact and negative capacitance. Paper presented at 2018 IEEE International Electron Devices Meeting (IEDM); December 1-5, 2018. San Francisco, CA. http://ieeexplore.ieee.org/stamp/stamp.jsp?tp=&arnumber=8614493&isnumber=8614478. Accessed January 17, 2019.
29. Ling ZP, Sakar S, Mathew S, et al. Black phosphorus transistors with near band edge contact Schottky barrier. *Sci Rep*. 2015;5:18000.
30. Kappera R, Voiry D, Yalcin SE, et al. Phase-engineered low-resistance contacts for ultrathin $MoS_2$ transistors. *Nat Mater*. 2014;13:1128-1134.
31. Pan Y, Dan Y, Wang Y, et al. Schottky barriers in bilayer phosphorene transistors. *ACS Appl Mater Interfaces*. 2017;9:12694-12705.

## SUPPORTING INFORMATION

Additional supporting information may be found online in the Supporting Information section at the end of this article.

**How to cite this article:** Lin Z, Wang J, Guo X, et al. Interstitial copper-doped edge contact for n-type carrier transport in black phosphorus. *InfoMat*. 2019;1:242–250. https://doi.org/10.1002/inf2.12015